Fuel 89 (2010) 1447–1460

Contents lists available at ScienceDirect

Fuel

journal homepage: www.elsevier.com/locate/fuel

Group combustion of staggeringly arranged heptane droplets at various Reynolds numbers, oxygen mole-fractions, and separation distances

Dongjo Lee [a], Ho Young Kim [a,*], Sam S. Yoon [a], Chong Pyo Cho [b]

[a] Department of Mechanical Engineering, Korea University, Anamdong, 5Ga, Sungbukgu, Seoul 136-701, Republic of Korea
[b] Automobile Energy and Environment Research Center, Korea Institute of Energy Research, 71-2 Jangdong, Yuseonggu, Daejeon 305-343, Republic of Korea

ARTICLE INFO

Article history:
Received 3 June 2009
Received in revised form 8 October 2009
Accepted 17 October 2009
Available online 5 November 2009

Keywords:
Group combustion
Staggered arrangement
Reynolds number
Separation distance
Oxygen mole-fraction

ABSTRACT

The group combustion of interacting heptanes liquid droplets are numerically simulated by solving two dimensional unsteady laminar Navier–Stokes equations. The unsteady computations for the time-varying vaporization of multi-droplets are carried out with parameters of the Reynolds number (*Re*), the separation distance (*S*) between the droplets, and the oxygen mole-fraction. The *n*-heptane droplets initially at T_0 = 300 K are in hot air of 10 atm at T_g = 1250 K. Multi-droplets are staggeringly arranged at a separation distance ranging from 4 to 15 droplet radius. The Reynolds number, based on the droplet diameter and free stream velocity, is varied from *Re* = 10 to 50. The oxygen mole-fraction of the surrounding air is changed from 15% to 90%. The time variations of the flame structure, the combustion characteristics, and the burning rates are presented and discussed. These results indicated that the staggered arrangement of the multi-droplets induced combustion characteristics distinct from those of a single droplet. The burning rate of the interacting droplets in the staggered arrangement exhibited a relatively strong dependence on the *Re*, *S*, and oxygen mole-fraction. The burning rate of the interacting multi-droplets, non-dimensionalized by that of a single droplet, was found as a function of *S* and *Re*.

1. Introduction

Understanding the vaporization and combustion processes of liquid fuel droplets is crucial for designing optimal combustion systems, particularly in IC-engines. In real sprays such as in furnaces, gas turbines, diesel engines and fire safety applications, liquid is injected into highly pressurized gas wherein droplets form and evaporate. This region of traveling droplets and high fuel vapor concentration is enveloped by a highly turbulent surrounding gas because of the hostile chamber environment (i.e., the injector's high pressure and spray's high speed). However, because these droplets are traveling as a group and the relative motion between droplets and gas within the envelope is quite small, this justifies the assumption of laminar flow inside this envelope.

In the real sprays, the local flow distribution around a droplet is non-spherical, non-symmetric, unsteady, multi-component, and closely-situated within a group combustion. Flow attacking a droplet is not typically uniform in thermo/physical properties and can retain significant fluctuation from the turbulent flow outside of the spray envelope. In such cases, the size of the turbulent eddy and length-scale should be properly taken into consideration (e.g., turbulence modeling). Buoyancy effects (e.g., Rayleigh–Taylor instability) of the fuel vapor at the droplet surface may also be important for some experiments. Gravity effects (e.g., Bond or Froud number) are generally assumed negligible, but may be pertinent in space applications. Because the droplets are subject to heat, surface tension is not uniform along the droplet surface, which may result in deformation of the surface shape (e.g., Weber number effect) and lead to surface-tension-driven oscillation, known as the Marangoni effect. Adding to the complexity, droplets are randomly dispersed with non-uniform separation distance yielding a constantly changing liquid volume fraction. In extreme cases, dense sprays may include binary collisions or/and coalescence that impact heat and mass transfer; droplet interactions may be sufficient to affect the physical properties of the gas in the region between droplets.

As such, modeling real spray combustion is an overwhelmingly complex process. However, increased computational power and the use of more complex models have facilitated steady progress towards the ultimate goal of simulating real spray combustion. Generally, an ideal droplet, (perfectly spherical and symmetric, quasi-steady, single-component, isolated droplet) is assumed for a simple analysis. As a step toward advancing modeling efforts, we consider multiple droplets in an ideal situation wherein all gas properties are uniform and laminar. Although these idealized droplets are far from a real scenario of a complex spray combustion problem, the analyses of these ideal droplets provide insight into

* Corresponding author. Tel.: +82 2 3290 3356; fax: +82 2 929 3082.
E-mail address: kimhy@korea.ac.kr (H.Y. Kim).

0016-2361/$ - see front matter © 2009 Elsevier Ltd. All rights reserved.
doi:10.1016/j.fuel.2009.10.015

and understanding of real spray combustion. Here, we also assume that inertia is the driving force that induces convective evaporation implying that the Reynolds number is the primary parameter significantly affecting the burning rate of multiple droplets. Because burning rate data are non-dimensionalized by the single droplet burning rate, we have a quantitative basis to compare multiple droplets a group-combustion scenario to the single droplet case. Such burn-rate information would be useful to automotive engineers with interest in how fuel droplet lifetime affects the fuel–air-ratio, which, in turn, affects the thermal efficiency and economical viability of the engine.

While extensive studies have been done to understand the burning of a single droplet [1–8], studies on group combustion of multiple droplets at various Reynolds numbers, oxygen mole-fractions, and the droplet separation distances are scarce. When droplets are closely spaced, the interaction of multiple droplets should not be overlooked. The effect of multiple droplets on combustion was previously investigated by Sirignano's group [9–12]. Chiu and his co-workers [13,14] explained that spray combustion regimes can be classified according to the group combustion number $G \sim 5N^{2/3}/k$, where N and k represent the total number of droplets in the cloud and the droplet separation parameter k, respectively (by assuming that Peclet number $\to \infty$). Here, k is proportional to the ratio between the droplet separation distance (S) and droplet diameter (d). Thus, G is large if k is small and the external group combustion regime is formed [13]. Conversely, if G is small because k is large, this yields the internal group combustion regime or individual burning of single droplets. The spray combustion behavior changes according to the following quantitative guideline: from (i) the external sheath regime, to (ii) the external group regime, to (iii) the internal group regime, to (iv) the single droplet regime, as G changes from $G > 100$, $100 > G > 0.1$, $0.1 > G > 0.01$, and $0.01 > G$, respectively. Our current numerical study is categorized as internal group regime (iii), $0.1 > G > 0.01$.

While previous studies pertain only to the vaporization process of multi-droplets, this work considers burning as well, along with the effects of other important characteristics such as separation distance, oxygen mole-fraction, and Reynolds number on the interacting burning droplets. Results should be particularly useful for investigating oxygen-enriched combustion [15], where adiabatic equilibrium flame temperature increases with higher oxygen mole-fraction, yielding reduced emissions. In theory, zero emission can be achieved with an oxidizer supply of 100% oxygen mole-fraction.

Heat and mass transfer arising from the relative motion between the droplets and gas is analyzed. In addition, Hill's vortex wherein re-circulation is observed due to the shear stress caused by the gas boundary layer at the droplet surface, is also modeled. We focus on the fundamental aspects of group combustion for an idealized array of constant-diameter droplets subject to uniform velocity and composition of the surrounding gas to better understand it's hydrodynamics and convective heating; vital information for the spray combustion community with relevance to many other applications. To our knowledge, nearly all group combustion modeling work assumes uniform ambient conditions, even at fairly high Reynolds numbers where ambient flow could be turbulent.

Two-dimensional flow over a bluff body at $Re = 40$ is simulated and the results are compared with previous data [14,16–17]. Then numerical validation of vaporizing droplets is carried out by computing the squared diameter of evaporating decane droplets and comparing simulations to the experimental data of Wong and Lin [7]. The results for single droplet burning are then compared to those of multiple burning droplets. The effects of the separation distance (S), Reynolds number (Re), and oxygen mole-fraction on multiple burning droplets are simulated and discussed. Finally, the overall results are summarized by plotting a contour map for the burning rate of multiple droplets on an S vs. Re plane.

2. Formulation

Fig. 1 shows the physical configuration of the present computation where droplets are staggered in convective environment. The droplet located at the lower left corner in the shaded box is referred to as the first droplet. In the counter-clockwise direction, the one at the lower right corner is referred to as the second droplet and the one at top is the third. These droplets form the enclosed "triangle" region. The fuel droplets are assumed to vaporize in a micro-gravity condition and in the forced convection environment. The thermal radiation effect is negligible because the vaporization of the droplets occurs at moderately low-temperature. Droplet deformation is also assumed to be minor under the moderate convection flow at $Re < 50$. The surface tension remains fairly constant despite the change in the liquid temperature.

The 2-D governing equations, listing conservation of mass, momentum, energy, and species, for the gas phase are given as follows:

$$\frac{\partial \rho}{\partial t} + \frac{\partial}{\partial x_i}\left\{\rho\left(u_i - \frac{\partial x_i}{\partial t}\right)\right\} = 0 \tag{1}$$

$$\frac{\partial}{\partial t}(\rho u_i) + \frac{\partial}{\partial x_j}\left\{\rho\left(u_i - \frac{\partial x_i}{\partial t}\right)u_j\right\} = -\frac{\partial P}{\partial x_i} + \frac{\partial}{\partial x_j}\left\{\mu\left(\frac{\partial u_i}{\partial x_j} + \frac{\partial u_j}{\partial x_i}\right)\right\} \tag{2}$$

$$\frac{\partial}{\partial t}(\rho h) + \frac{\partial}{\partial x_j}\left\{\rho\left(u_j - \frac{\partial x_j}{\partial t}\right)h\right\} = \frac{\partial}{\partial x_j}\left(\frac{k}{c_p}\frac{\partial h}{\partial x_j}\right) + \sum_{n=1}^{N} h_{0k} v_k \omega_k \tag{3}$$

$$\frac{\partial}{\partial t}(\rho Y_k) + \frac{\partial}{\partial x_j}\left\{\rho\left(u_j - \frac{\partial x_j}{\partial t}\right)Y_k\right\} = \frac{\partial}{\partial x_j}\left(\rho D_k \frac{\partial Y_k}{\partial x_j}\right) - v_k \omega_k \tag{4}$$

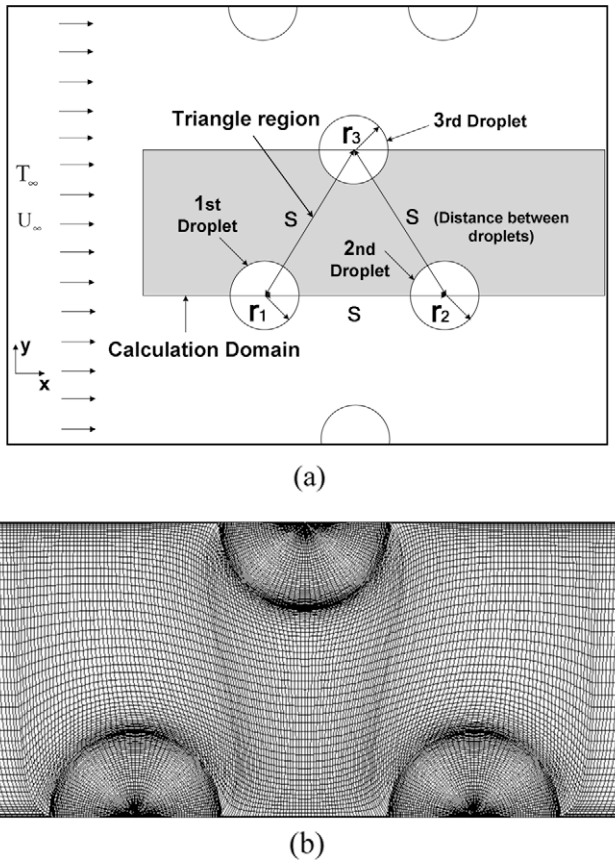

Fig. 1. Schematic (a) and grid (b) of fuel droplets burning in a convective flow.

where $\rho, u, \mu,$ and P are the density, velocities, viscosity, and pressure. Enthalpy and thermal conductivity are expressed in terms of h and k. The symbols h_{0k}, D_k, Y_k, $v_k, and \omega_k$ represent the enthalpy of formation, diffusion coefficient, mass fraction, and mass production or consumption rate of species $()_k$, respectively. The term, $\partial x_i/\partial t$, accounts for the conservation of mass during the variation in grid adjustment due to droplet evaporation; droplet size is reduced when evaporation occurs.

The equation of state of Peng–Robinson [18] is used. Here, a single-step global finite-rate chemical reaction is applied to simulate n-heptane combustion. The stoichiometric of n-heptane oxidation is written as below:

$$C_7H_{16} + 11(O_2 + 3.76N_2) \rightarrow 7CO_2 + 8H_2O + 41.36N_2 \quad (5)$$

The reaction rate ($\dot{\omega}$) of Westbrook et al. [19], is given as below:

$$\dot{\omega} = 2.868 \times 10^9 \, W_{fu} [C_7H_{16}]^{1/4} [O_2]^{3/2} \exp(-15098/T) \quad (6)$$

As for the liquid phase, the following mass, momentum, and energy governing equations are used:

$$\frac{\partial \rho}{\partial t} + \frac{\partial}{\partial x_i}\left\{\rho\left(u_i - \frac{\partial x_i}{\partial t}\right)\right\} = 0 \quad (7)$$

$$\frac{\partial}{\partial t}(\rho u_i) + \frac{\partial}{\partial x_j}\left\{\rho\left(u_i - \frac{\partial x_i}{\partial t}\right)u_j\right\} = -\frac{\partial P}{\partial x_i} + \frac{\partial}{\partial x_j}\left\{\mu\left(\frac{\partial u_i}{\partial x_j} + \frac{\partial u_j}{\partial x_i}\right)\right\} \quad (8)$$

$$\frac{\partial}{\partial t}(\rho c_p T) + \frac{\partial}{\partial x_j}\left\{\rho c_p\left(u_j - \frac{\partial x_j}{\partial t}\right)T\right\} = \frac{\partial}{\partial x_j}\left(k\frac{\partial T}{\partial x_j}\right) \quad (9)$$

where T and c_p are the temperature and specific heat, respectively.

Table 1
Evaluation of the thermo-physical properties.

Properties	Method
ρ_l	Rackett [27]
k_l	Latini and Pacetti [28]
μ_l	Sastri–Rao method [29]
$c_{p,l}$	Corresponding states methods (CSP) [30]
L	Watson relation [31]
$c_{p,g}$	Abramzon and Sirignano [32], Wilke's method [33]
μ_g	Lucas [34], Lucas mixing rule [35]
k_g	Abramzon and Sirignano [32], Wilke's method [33]
D_g	Fuler et al. [36]

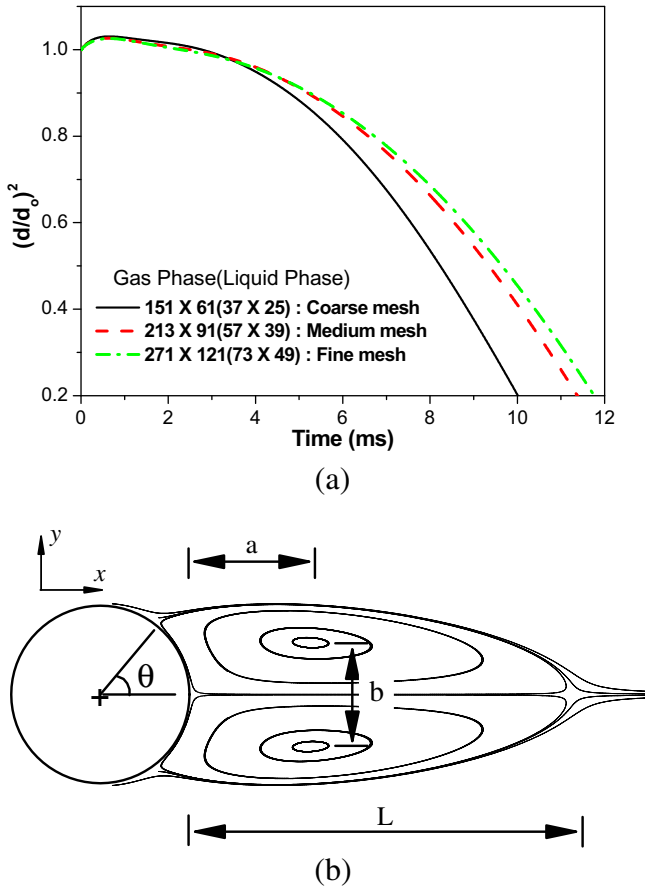

Fig. 2. Variation of diameter-squared obtained by various numerical grids (a) and streamlines obtained by the present calculation for $Re = 40$ and definition of wake parameters (b).

Table 2
Model results compared to previous research for $Re = 40$.

	Constanceau and Bouard [23]	Rengel and Sphaier [24]	Wanderley and Levi [25]	Present study	Standard deviation
C_d	N.A.	1.61	1.60	1.65	0.022
L/D	2.13	2.23	2.10	2.16	0.048
a/D	0.76	0.72	0.69	0.69	0.029
b/D	0.59	0.58	0.58	0.59	0.005
θ	53.50	54.06	53.20	53.55	0.309

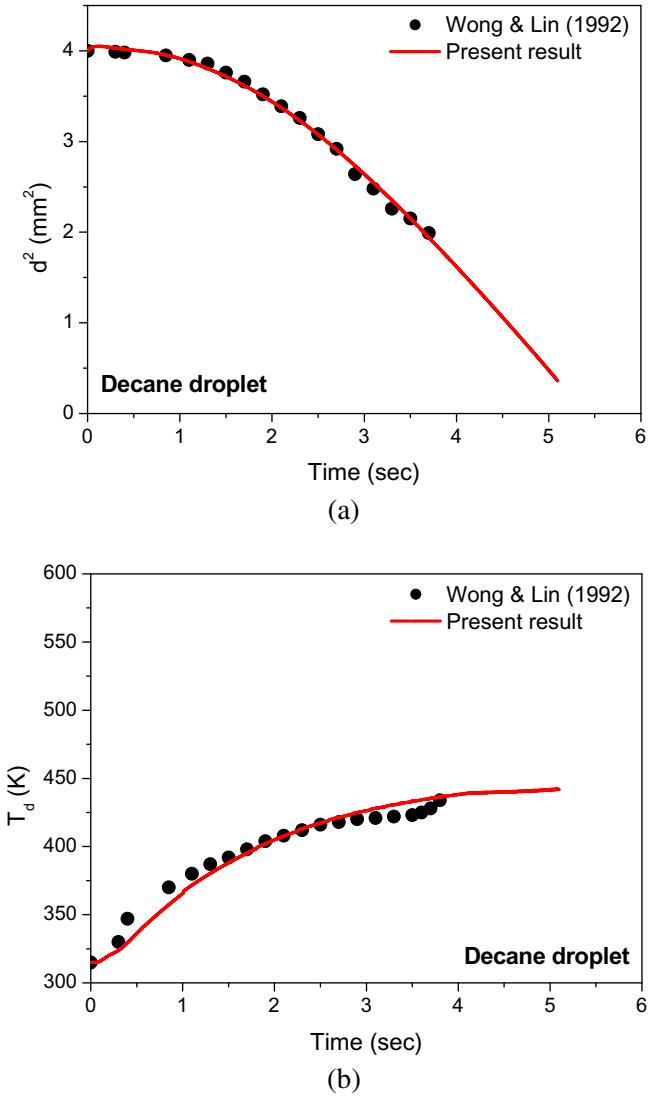

Fig. 3. Comparison with numerical and experimental [7] of single droplet (a) diameter-squared and (b) temperature results for decane droplet.

The initial conditions are:

$$u_g = u_\infty, T_g = T_\infty, Y_o = Y_{o,\infty}, Y_f = Y_{f,\infty}, T_l = T_o$$

Because of the symmetry at $y = 0$, all gradients at the centerline are zero. Other boundary conditions are included as follows:

(a) At the droplet center ($r = 0$)

$$v_l = \frac{\partial \phi}{\partial n} = 0 \quad \text{where} \quad \phi = u_l,\ T_l,\ Y_f \tag{10}$$

(b) At the droplet surface ($r = r(t)$)

$$u_{l,s} = u_{g,s}, \tau_{l,s} = \tau_{g,s}, T_{l,s} = T_{g,s}$$

$$\dot{m}'' = Y_f \dot{m}'' - \rho_g D_g \left(\frac{dY_f}{dn}\right)_s \tag{11}$$

$$\left(k\frac{\partial T}{\partial n}\right)_{g,s} = \left(k\frac{\partial T}{\partial n}\right)_{l,s} + \dot{m}'' L \tag{12}$$

$$u_n = \frac{\dot{m}''}{\rho_{g,s}} - \frac{dr}{dt} \tag{13}$$

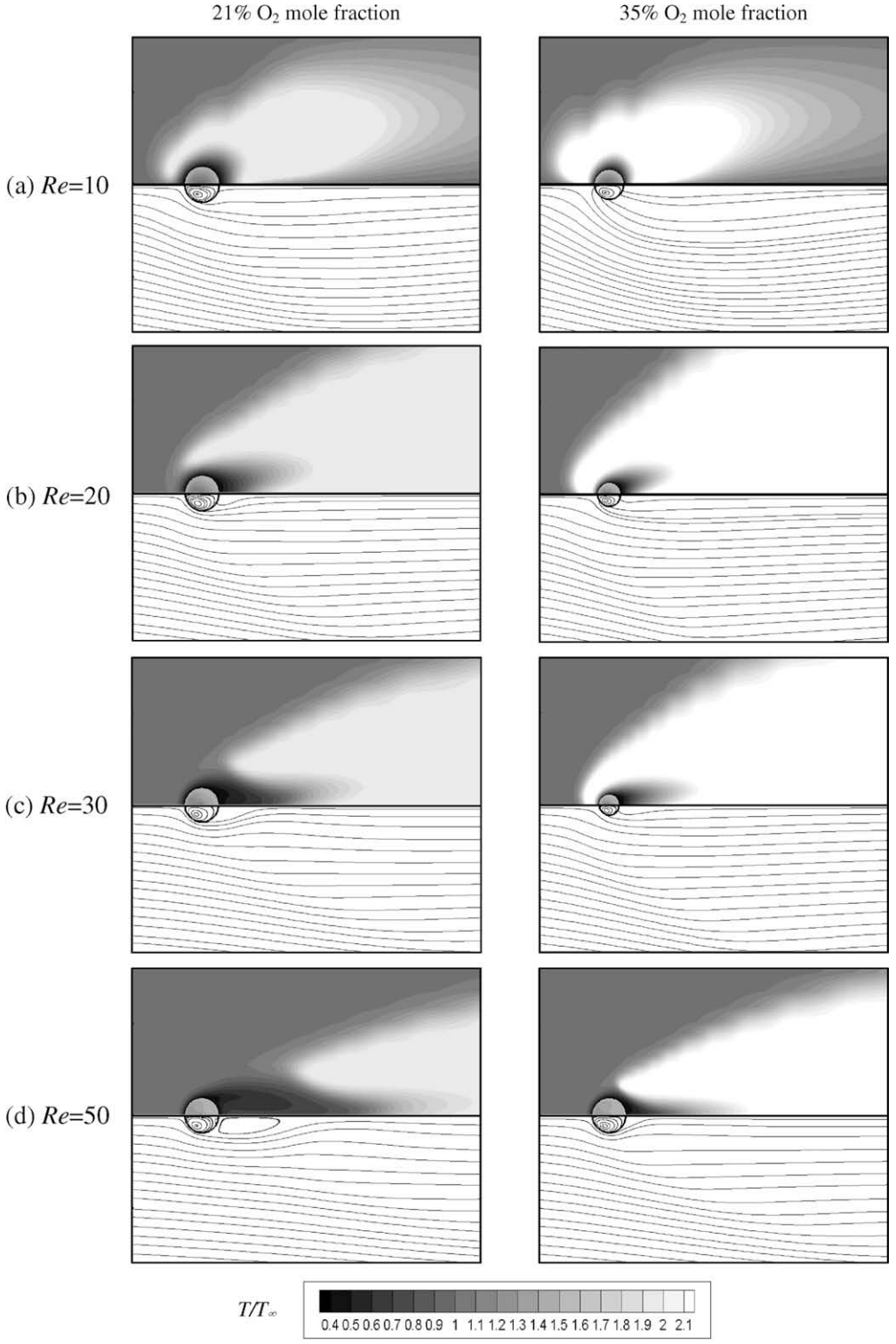

Fig. 4. Snapshots of the isotherms and streamlines of the liquid and gas phases taken at $t = 6$ ms during the single droplet burning.

where $\dot{m}''$, L, and u_n are the total mass flux on the surface, latent heat, and blowing velocity. The film theory of Cussler [20] for computing the total mass flux of the gas mixture is employed. The fuel vapor mole-fraction at the droplet surface can be obtained by using the Wagner equation [21] to estimate the vapor pressure. This Wagner equation below is particularly suitable for high temperature applications:

$$\ln P_{vp_r,s} = (a\tau + b\tau^{1.5} + c\tau^{2.5} + d\tau^5)/T_r \quad (14)$$

Here, T_r and $P_{vp_r,s}$ are the reduced temperature and fuel vapor pressure. The relevant relations and constants are defined as below:

$$P_{vp_r,s} = P_{vp,s}/P_c, \quad \tau = 1 - T_r, \quad T_r = T_s/T_c \quad (15)$$

$$a = -8.04937, b = 2.03865, c = -3.312, d = -3.648 \quad (16)$$

From the results above, we obtain the following relation:

$$Y_{fu,s} = \frac{P_{vp,s}}{P_{ref}} \frac{MW_{fu}}{\sum_i x_i MW_i} \quad (17)$$

The methods that are used to evaluate the thermo-physical properties are summarized in Table 1. At the droplet interface, mass flux is calculated by diffusion theory, which includes the effects of diffusion-induced convection and that of the moving interface, instead of classical film theory [9]. The diffusion time ($t = d_0^2/D_g$) is chosen to select the time scale representing the diffusion velocity. The present results obtained using the diffusion theory showed good agreement with those obtained using the classical film theory [9].

The governing equations of gas and liquid phases are discretized into their algebraic counterparts based on the finite-volume method. The SIMPLEC algorithm [22] is applied to solve the flow field of the gas and liquid. The power-law scheme is implemented to solve the convective and diffusive terms in the Navier–Stokes equations. The second order implicit scheme is utilized to advance all variables in time.

3. Numerical verification and validation

The computational domain comprises several blocks of mesh. The mesh for the droplets are timely adjusted so that the time integral of the mass, momentum, and energy transfer between

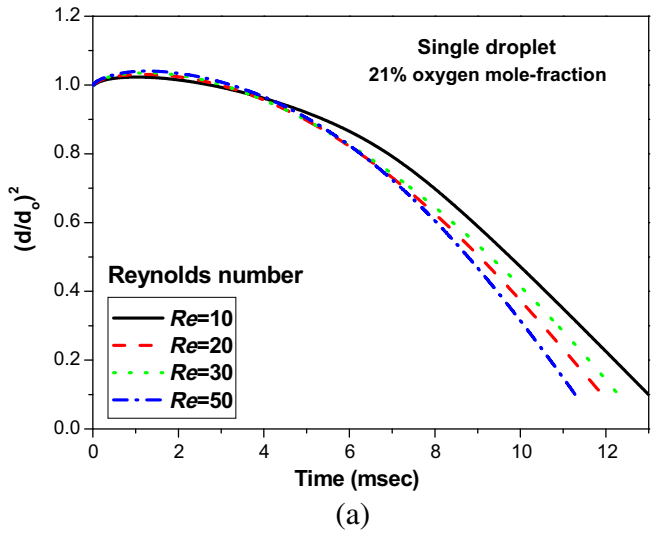

Fig. 5. Histories of the single droplet diameter-squared (a) at various Reynolds numbers with 21% oxygen mole-fractions and (b) at various oxygen mole-fractions with Re = 10.

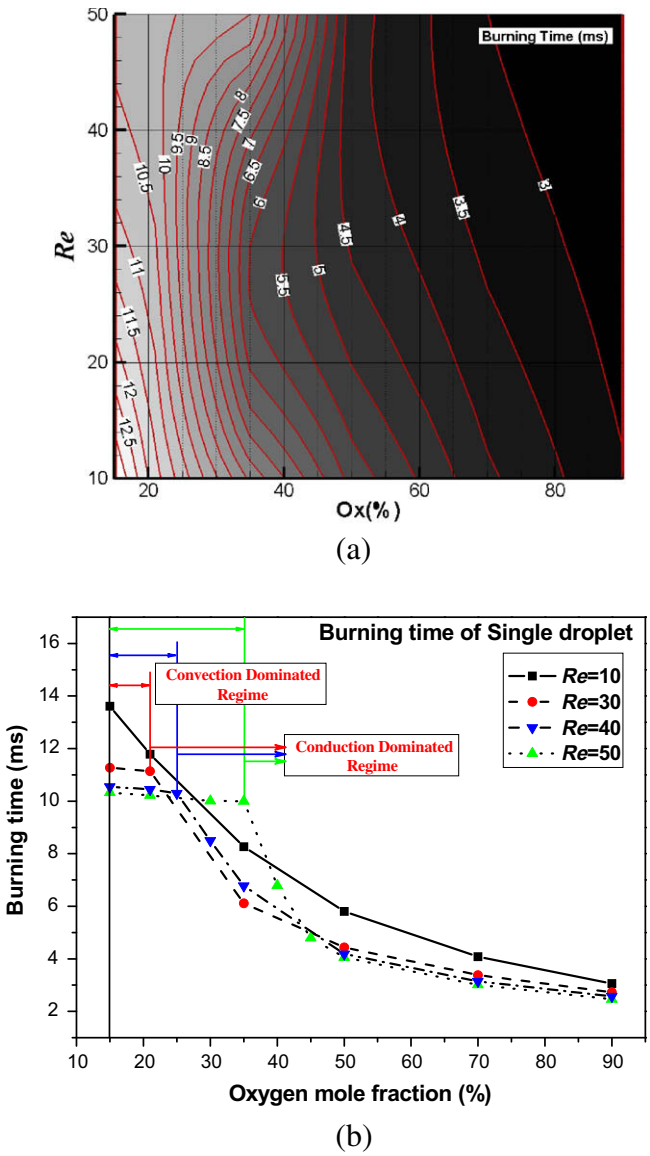

Fig. 6. Burning time (t_b, in millisecond) of a single droplet as a function of oxygen mole-fraction (O_2%) and Reynolds number (a) on a contour plot and (b) on a t_b vs. O_2% plot.

the liquid and gas phases is accurately incorporated. As for the computational details, the mesh resolutions of 57×39 and 213×91 are used for the liquid and gas phases, respectively. These mesh resolutions seem to produce convergent results for the droplet vaporization rate, as shown in Fig. 2a. Prior to simulating droplet combustion, a simple numerical verification procedure is carried out by calculating the flow around a 2D cylindrical case. Results obtained with the current code are compared with those presented in Refs. [23–25]. The operating Reynolds number was $Re = Ud/\nu = 40$, where d is the cylinder diameter. Here, a, b, L, and θ are the centers of the vortices in the x- and y-direction, the vortices size, and the separation point, as shown in Fig. 2b (this figure shows the actual computed streamlines). The comparisons indicated that the current code is capable of predicting results within 0.1–4.2% error, based on the standard deviation, as shown in Table 2.

For a vaporizing droplet, the computed results were compared with the diameter-squared history of a vaporizing decane droplet of Wong and Lin [7]. Wong and Lin measured both the droplet size and the temperature evolution of the droplet under a relatively high evaporative condition. The initial conditions of their decane droplet were $d_0 \approx 2$ mm and $T_{d,0} = 315$ K; the droplets were exposed to a high temperature moving air stream with $T_g = 1000$ K and $Re_0 = Ud_0/\nu = 17$. Moreover, the thermocouples placed inside the suspended droplet were used to measure the histories of the droplet temperature at different locations. Comparisons of the droplet's vaporizing characteristics with the present results are provided in Fig. 3; Wong and Lin measured the internal local temperature of the decane droplet at $r/r_0 = 0.6$, inside the droplet. A time step of $\Delta t \approx 1$ ms is used in this study. This comparison indicated that the present results are in excellent agreement with the experimental data. One noticeable behavior is that the droplet heat-up period, in which the nonlinear behavior of d^2 with respect to time is shown, occupies a fairly large portion of the entire lifetime of the droplet.

4. Results and discussions

4.1. Single droplet burning

A single droplet initially at the temperature of $T_0 = 300$ K was situated within hot air flow of 10 atm and $T_\infty = 1250$ K and oxygen mole-fractions ranging between 15% and 90%. The Reynolds number, based on the droplet diameter ($d_0 = 100$ μm) and properties, was changed from $Re = 10$ to 50.

The ignition temperature of n-heptane fuel vapor at 10 atm environment is 463 K [26]. During our simulation, modeling flash ignition is not necessary as the droplet temperature gradually increases according to the kinetically controlled reactions of the

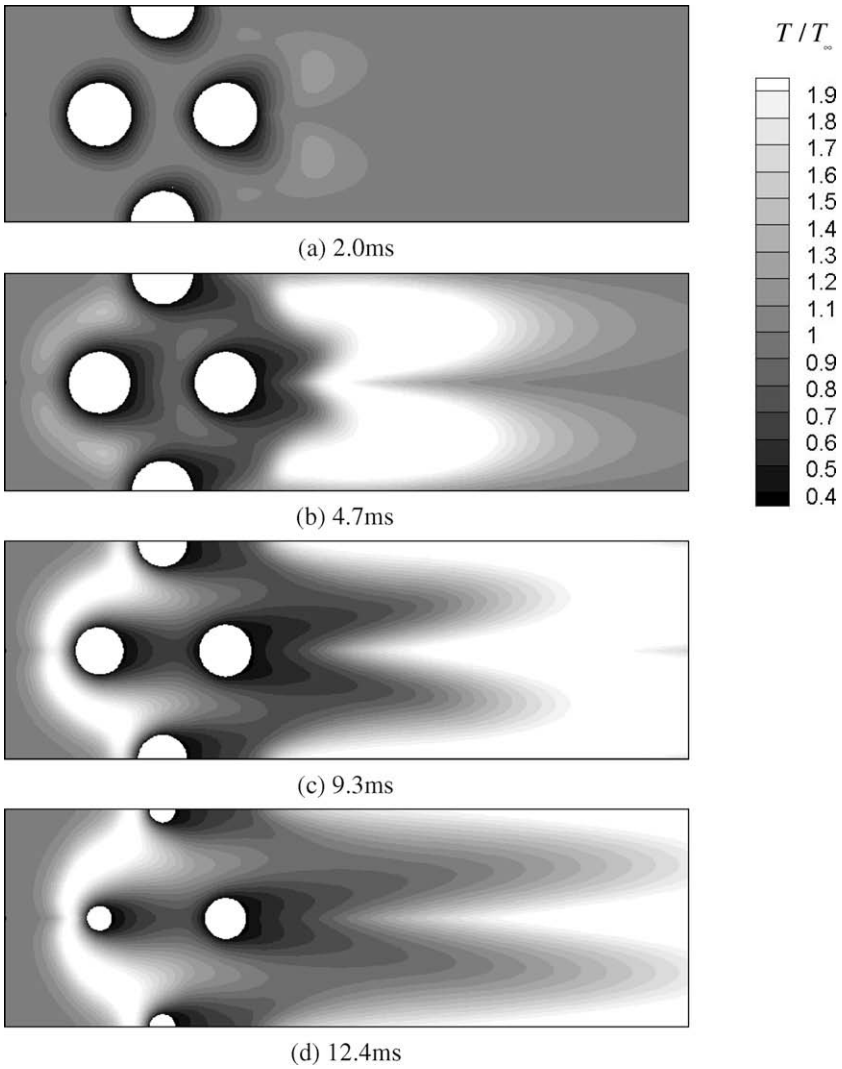

Fig. 7. Snapshots of the flame configuration at $S/r_0 = 4$, $Re = 10$, and 21% oxygen mole-fraction.

Arrhenius model. This reaction rate is governed by the gas temperature and species concentration and is irrelevant to the ignition temperature of the *n*-heptane.

The isotherms and streamlines of both liquid and gas phases during the single droplet burning in the range of $10 \leqslant Re \leqslant 50$ at given 21% and 35% oxygen mole-fractions are shown in Fig. 4. The streamlines indicate that the Hill's vortex is developed within the droplet even at the quite small Reynolds number of $Re = 10$. At $Re \leqslant 20$, in which the heat transfer effect is dominant over the droplet's vaporization process, a relatively large flame enclosing the droplet appears at both 21% and 35% oxygen mole-fractions. Generally, the higher oxygen mole-fraction, the shorter the lifetime of a droplet for most Reynolds numbers, except for $Re = 50$. When the Reynolds number is fairly high, and thus the convective vaporization is dominant, the higher oxygen mole-fraction of 35% does not necessarily guarantee faster burning than the 21% oxygen mole-fraction.

Fig. 5 show the effect of the Reynolds number for the 21% oxygen mole-fraction and the effect of the oxygen mole-fraction for the $Re = 10$ on the lifetime of a heptane single droplet. In Fig. 5a, The heating period lasted until $t \sim 4$ ms, after which the vaporization rate became linearly stiff. During this period, the droplet size becomes greater than the original size because of the droplet's sudden exposure to hot gas, which induces temporary swelling. As shown, the droplet lifetime is shortened with increasing Reynolds number, except for $Re = 30$. This phenomenon is explained by the competition between convection and the heat added by the surrounding flame. For example, when the Reynolds number is low (i.e., $Re = 10$), convection is not strong enough to drift away the flame that envelopes the droplet. When it is increased to $Re = 20$,

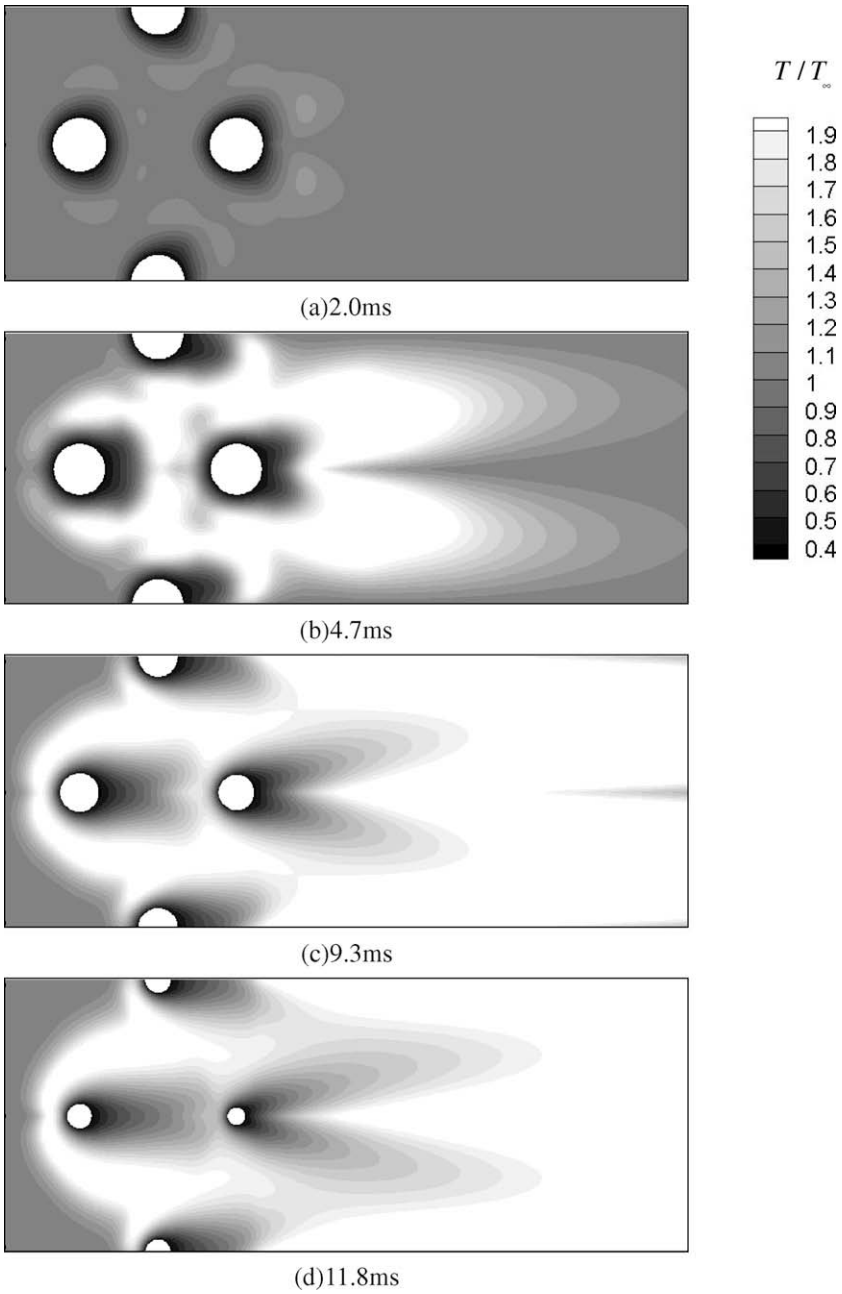

Fig. 8. Snapshots of the flame configuration with time at $S/r_0 = 6$, $Re = 10$, and 21% oxygen mole-fraction.

convection is moderate enough to expedite the vaporization process and, thus, the droplet's lifetime is shortened. In this case of $Re = 20$, the enveloping flame is still responsible for enhancing the droplet's vaporization process because of its closer location to the droplet. However, when the Reynolds number is further increased to $Re = 30$, the hot flame is drifted downstream so the flame no longer has prominent influence of heat addition to the vaporization process. In such case of $Re = 30$, convection is the dominant mechanism that drives the vaporization, which results in slower burning than the burning in the case of $Re = 20$; the droplet's lifetime, therefore, increases when the Reynolds number is changed from $Re = 20$ to 30. Eventually, when the vaporization process is dominated by convection as in $Re = 50$, the vaporization rate is the highest. Fig. 5b shows the effect the oxygen mole-fraction on the lifetime of the heptane single droplet. As the oxygen mole-fraction is increased, the linear rate of burning, which initiates as early as $t = 1.3$, 1.7, 2.5, 3.5, and 6.0 ms for corresponding 90%, 70%, 50%, 30%, and 21% O_2 mole-fractions, becomes stiffer (having more rapid vaporization rate). The instant times, $t = 1.3$, 1.7, 2.5, 3.5, and 6.0 ms, recorded here is when the diameter-squared history begins to deviate from that of the 15% O_2 result. This increased vaporization rate with greater oxygen mole-fraction is explained by the increase in the adiabatic equilibrium flame temperature. A greater flame becomes closely-situated around the droplet with increasing oxygen mole-fraction, as shown in Fig. 4.

Fig. 6 shows the burning time (t_b) of a single droplet as a function of the oxygen mole-fraction (O_2%) and Reynolds number on a contour plot and on a t_b vs. O_2% plot in Fig. 6a and b, respectively. It is fair to say, in general, that the burning of a single droplet is predominantly influenced by the oxygen mole-fraction rather than the Reynolds number. At relatively high oxygen mole-fraction of approximately 50% or greater, the Reynolds number has more influence on convective vaporization; the higher the Reynolds number, the faster the vaporization process and the lesser the burning time. On the other hand, at a relatively moderate oxygen mole-fraction ranging approximately $25\% < O_2 < 45\%$, the burning time becomes the largest at the intermediate Reynolds number of $Re \sim 25$ or 30. In this regime of moderate oxygen mole-fraction, two driving vaporization mechanisms of convection and flame heat addition are competing against each other. At fairly a low oxygen mole-fraction of 20% or less, the Reynolds number influence is again prominent as the burning time decreases with larger Re. Fig. 6b shows the burning time as a function of oxygen mole-fraction at various Reynolds numbers, providing additional insights on the effects of O_2 and Re. At $Re = 10$, a moderately smooth decrease in the burning time is observed with increasing oxygen mole-fraction. At the low Reynolds number of $Re = 10$, a flame surrounds the single droplet and becomes bigger and more active with more oxygen supply; here the heat addition by surrounding flame is dominant. However, as Re increases, the burning time changes rather abruptly at around $21\% < O_2 < 35\%$ and $35\% < O_2 < 50\%$ for $Re = 30$ and 50, respectively. Interestingly, at 35% O_2, the burning time of $Re = 50$ is greater than that of smaller $Re = 10$ and 30. In this relatively high Re regime, the convection effect barely holds the flame downstream, so reduced heat is provided to the droplet, which in turn induces slower vaporization. This pattern persists only up to about 35% O_2, beyond which any greater oxygen supply yields a vaporization condition that is completely controlled by the oxygen mole-fraction only; the convection effect is meager when oxygen mole-fraction is too high. This explanation is applicable and manifested in the pattern shown in Fig. 6a; one may see a stiff gradient of the contour level for $35\% < O_2 < 50\%$ at $Re = 50$. This stiff gradient is shown in the range of $21\% < O_2 < 35\%$ for $Re = 30$.

In general, a droplet would have a shorter lifetime with a higher Reynolds number during the convection-dominated flow; the larger the flow velocity, the higher the evaporation rate. This is true only when there is no other competing factor which alters the evaporation rate. When other factors, such as heat addition via

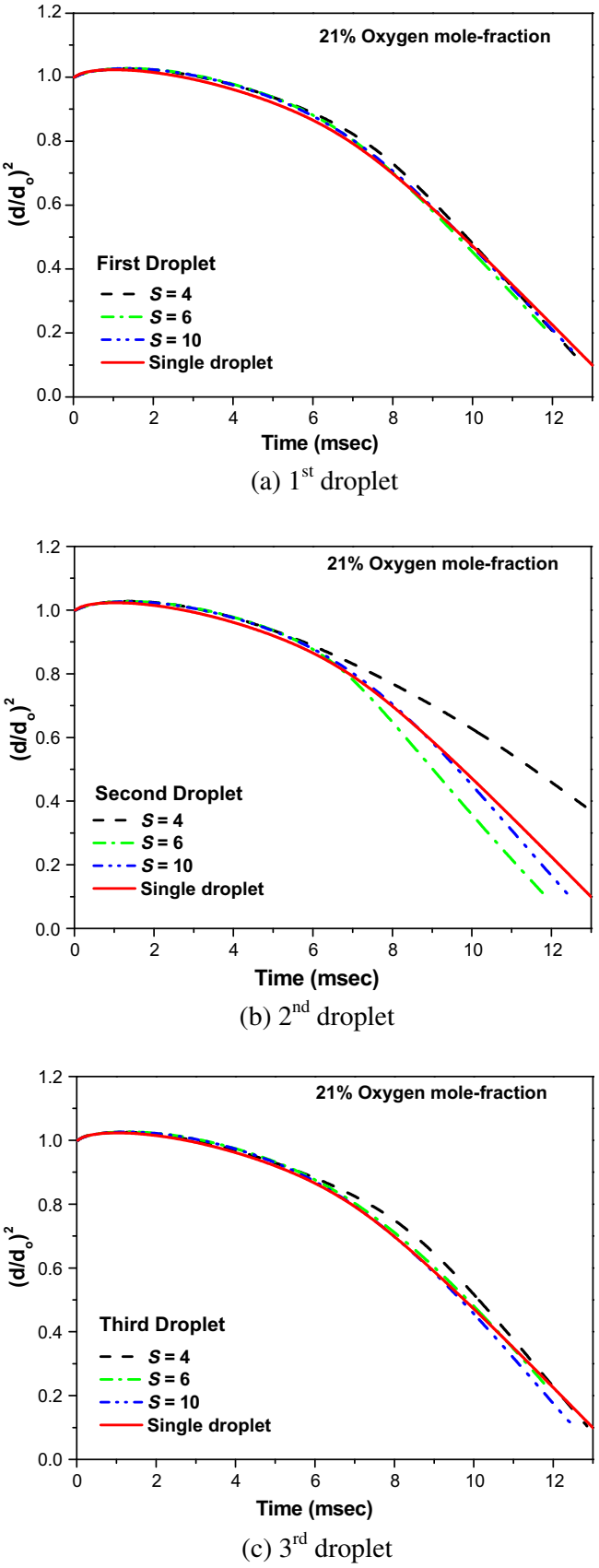

Fig. 9. Histories of the multiple droplet diameter-squared at various separation distance, S. The Reynolds number is fixed at $Re = 10$.

conduction from the flame, play a competing role against the convection effect, there exists a sudden regime change as shown in Fig. 6b. This regime change occurs at different critical O_2 mole-fraction for different Reynolds numbers. At a lower oxygen mole-fraction, convection effect tends to dominate; Fig. 6b shows this convection-dominated effect as the burning time is smaller with the larger Reynolds number. This convection-dominated regime persists up to a critical O_2 mole-fraction, beyond which the conduction effect plays a major role. Because of the flame approaching the droplet with an increasing O_2 mole-fraction, rapid evaporation occurs; Fig. 4 shows this trend. It should be reminded that, at larger *Re*, the "hot flame" tends to locate further downstream because of stronger convection; this results in a reduced addition via conduction. For this reason, it would take sufficient amount of oxygen for the flame to situate closely around the droplet. In other words, it takes larger oxygen mole-fractions for the regime change to occur when the Reynolds number is large, having larger convection-dominated regime as shown in Fig. 6b.

4.2. Multi-droplets burning: effect of separation distance

The multiple droplets initially at the temperature of $T_0 = 300$ K were situated within hot air flow of 10 atm and $T_\infty = 1250$ K with various oxygen mole-fractions that range from 15% to 90%. The multiple droplets are staggeringly arranged with the separation distance (S) that ranges from $S/r_0 = 4$ to 15, forming a triangle region, as shown in Fig. 1. The Reynolds number, based on the droplet diameter ($d_0 = 100\mu m$) and properties, is changed from $Re = 10$ to 50.

Fig. 7 shows the snapshot of the flame configuration for $Re = 10$ and $S/r_0 = 4$ at 21% oxygen mole-fraction. As time increases, the droplets vaporize, and then, the vapor ignites and a high temperature flame appears behind the droplets. At a later time of $t \geqslant 9.3$ ms, the flame eventually envelopes the fronts of the first and third droplet. It seems that the first droplet burns at the fastest rate because of the hot flame in the front; which adds substantial heat to the first droplet. As for the second droplet, the fuel vapor of relatively low temperature emitted and drifted from the first droplet prevents the second droplet from burning efficiently. Moreover, the staggered location of the third droplet also circumvents the fuel vapor from being convected downstream, leading to an accumulation of the fuel vapor inside the triangle region. It is interesting that this pattern of slower burning of the second droplet is completely reversed when the separation distance is increased from $S/r_0 = 4$ to 6, as in Fig. 8.

In Fig. 8, the second droplet burns faster than the first and third droplets. The larger space between droplets allows sufficient oxygen supply into the triangle region holding the hot flames. Because of these flames from the upstream, the second droplet vaporizes and burn at a faster rate. Furthermore, accelerated flow between droplets also helps to enhance convection to the second droplet, and this enhanced convection leads to faster vaporization and burning processes. Unless the separation distance is very small (i.e., $S/r_0 < 5$), the second droplet generally burns faster than the first and third droplets for most oxygen mole-fractions.

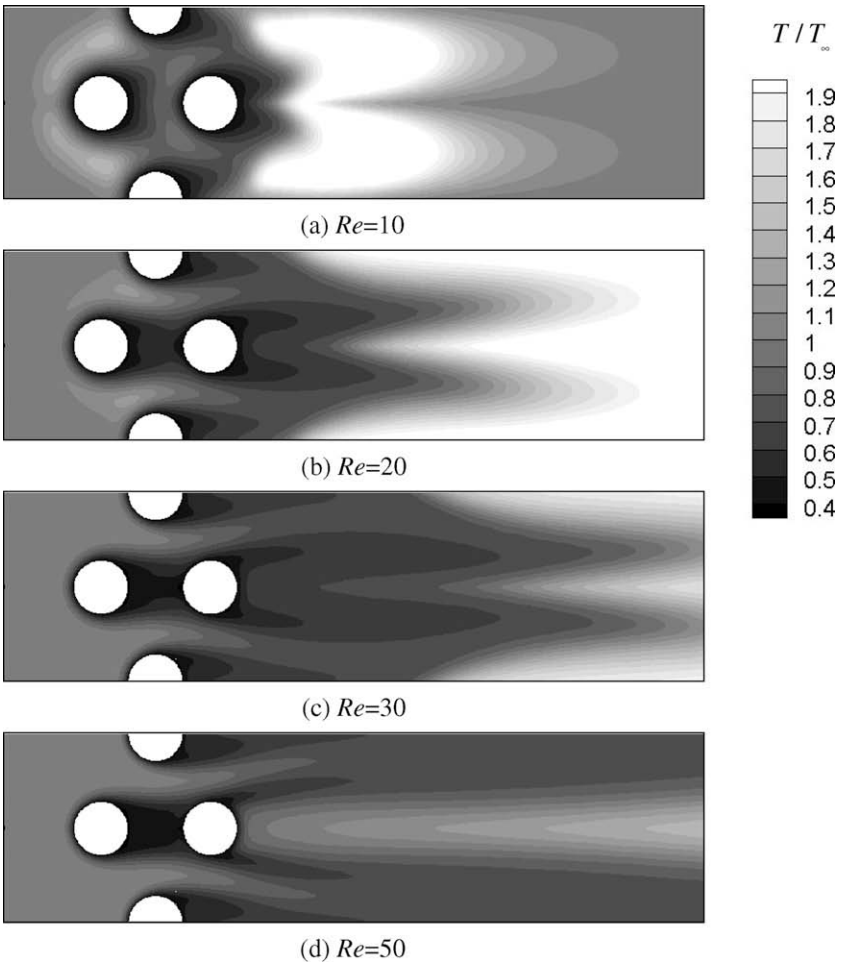

Fig. 10. Effect of the Reynolds number: snapshots of the flame configuration taken at $t = 4.7$ ms, $S/r_0 = 4$, and 21% oxygen mole-fraction.

The history of the droplet size as a function of S is shown in Fig. 9. The results of the first, second, and third droplets are compared with that of the single droplet. As shown, the lifetimes of the first and third droplets are fairly constant and insensitive to S. However, discernable deviation of the lifetime of the second droplet begins to appear at around $t \sim 7$ ms with variation of S. As mentioned, the slower vaporization process of the second droplet at small S (i.e., $S/r_0 = 4$) is due to the down-streaming of the low-temperature vapor from the first and third droplets. However, as the distance is increased to $S/r_0 = 6$, the second droplet burns faster because the second droplet is directly exposed to the flame that infiltrated the triangle region, and consequently, the vaporization process of the second droplet is expedited. As S is further increased from $S/r_0 = 6$ to 10, the burning rate of the second droplet is slowed again because the flame from the first droplet does not maintain its prominent influence, and the burning characteristic of multi-droplets converges to that of the single droplet, as it should as S approaches infinity.

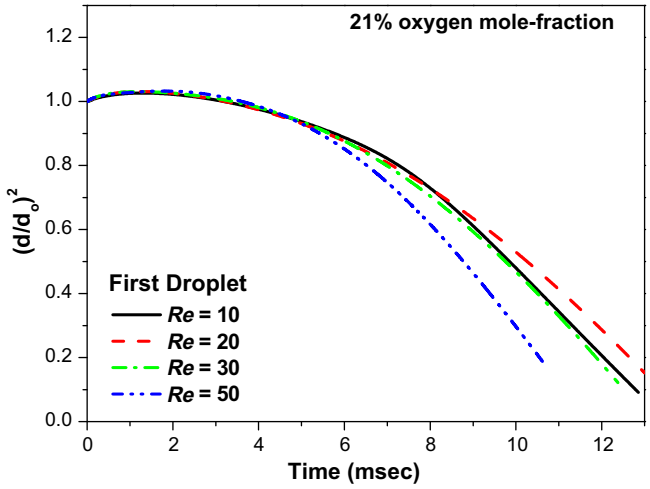

(a) 1st droplet

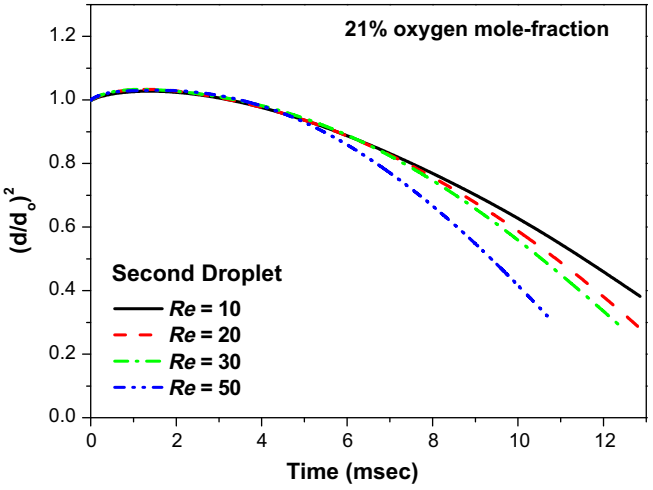

(b) 2nd droplet

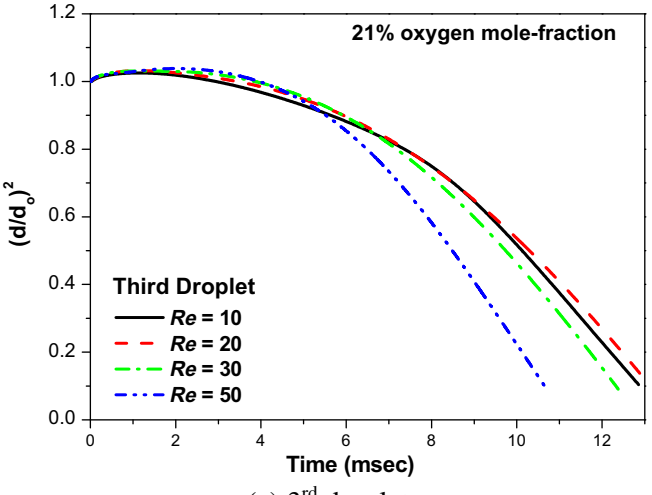

(c) 3rd droplet

Fig. 11. Histories of the multiple droplet diameter-squared at various Reynolds numbers. The separation distance and the oxygen mole-fraction are fixed at $S/r_0 = 4$ and 21%.

4.3. Multi-droplets burning: effect of Reynolds number

Here, the effect of the Reynolds number on the vaporization and burning processes of multi-droplets is studied. The Reynolds number of our interest in the laminar flow ranged from $Re = 10$ to 50. Fig. 10 shows the snapshots of the multi-droplets burning at fairly small $S/r_0 = 4$ at 21% oxygen mole-fraction taken at $t = 4.7$ ms. The larger the Reynolds number, the further the hot flame located from the droplets, as shown in Fig. 10. Fig. 11 quantitatively compares the histories of all three droplets at various Reynolds numbers. The first and third droplets retain a similar history pattern as that

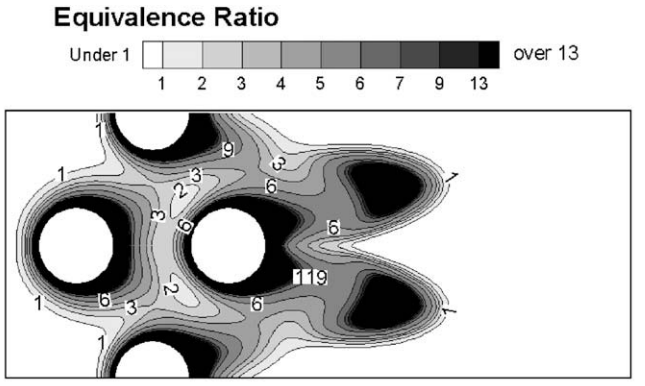

(a)

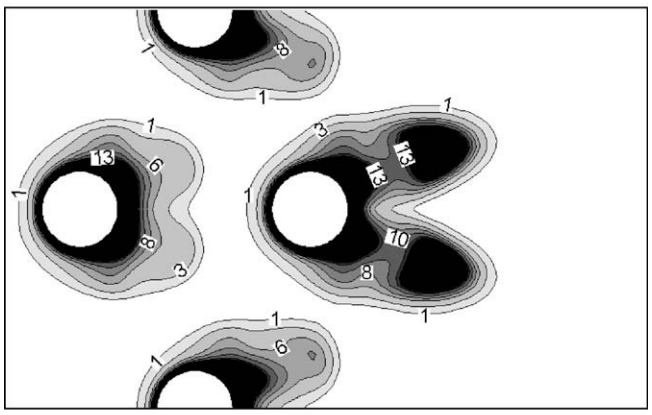

(b)

Fig. 12. Comparison of the equivalence ratio distribution at the separation distance of (a) $S/r_0 = 4$ and (b) and $S/r_0 = 6$. The Reynolds number and oxygen mole-fraction are fixed at $Re = 10$ and 21%. The snapshots of the equivalence ratio distribution taken at $t = 4.7$ ms.

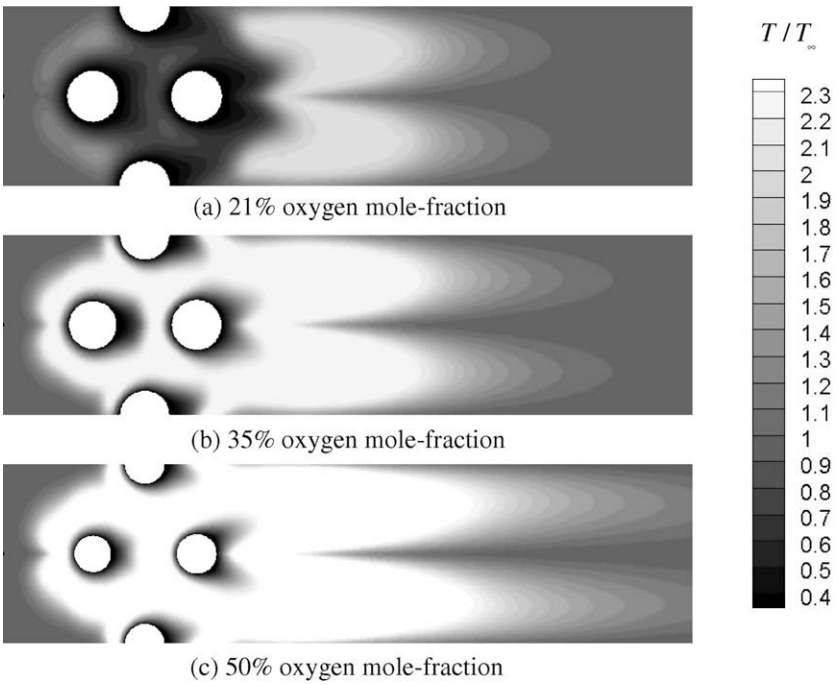

Fig. 13. Effect of the oxygen mole-fraction: snapshots of the flame configuration taken at $t = 4.7$ ms, $S/r_0 = 4$ and $Re = 10$.

of the single droplet shown in Fig. 5a. The increase in the Reynolds numbers from $Re = 10$ to 20 surprisingly lengthens the lifetime of the first and third droplets because of the reduced addition of heat by the hot flame shift. It is noted that, at these low Reynolds numbers of $Re \leqslant 20$, bulk of the vaporization process is dominated conduction rather than convection due to the presence of the hot flames. However, when the Reynolds number increases from $Re = 20$ to 30, the convection effect begins to dominate, and eventually, at $Re = 50$, the vaporization of the first and third droplets is greatly shortened. As for the effect of Reynolds number on the second droplet behavior, the accumulated low-temperature vapor in the triangle region plays an important role in the vaporization process of the multiple droplets. This low-temperature vapor effect is prominent especially when the separation distance, S, is small. It is reminded that it is difficult for the hot flame to be smeared inside the triangle region at this small value of S. Thus, the larger the Reynolds number, the stronger the convective force that can further drift the vapor downstream and increase the vaporization process of the second droplet; this explanation is consistent with what is observed in Fig. 11b. The ratio of fuel to air concentration is plotted in Fig. 12, indicating that relatively higher fuel concentration centers around the second droplet at smaller value of $S/r_0 = 4$; compare Fig. 12a and b.

4.4. Multi-droplets burning: effect of oxygen mole-fraction

Fig. 13 shows the snapshots of the burning of multi-droplets at various oxygen mole-fractions and Fig. 14 shows the quantitative comparison of the lifetime of multi-droplets with that of the single droplet at various oxygen mole-fractions of 21%, 35%, and 50%. As expected, lifetime is substantially reduced for all three droplets at higher oxygen mole-fractions. Generally, the multi-droplets tend to burn at a slower rate than the singe droplet for most oxygen mole-fractions when the separation distance is reasonably small, exhibiting group combustion characteristics. This relatively slower burning of multiple droplets, as compared to that of the single droplet, is attributed to the accumulated low-temperature vapor in the triangle region at small values of S. However, it should be noted that the vaporization process of the second droplet would be substantially expedited by hot temperature flames that infiltrate the triangle region when S is increased. The lifetime of the first droplet is comparable to that of the single droplet. If the burning rate is ranked according to speed, the burning rate of the first droplet is at the fastest (because of its similarity to the single droplet) followed by the third and the second droplet (which is most influenced by the major parameter of group combustion, S).

4.5. Summaries on multi-droplets burning time

The dimensionless burning rates of the first, second and third droplets, non-dimensionalized by the single droplet burning rate, are plotted on a two-dimensional plane of S and Re for 21% and 35% oxygen mole-fractions in Fig. 15. The burning rate of the single droplet, used for non-dimensionalizing the multi-droplet burning rate, is obtained at "all" corresponding values of Re at given 21% and 35% oxygen mole-fractions. Because the contour variable is the burning rate, the higher burning rate indicates faster vaporization and thus the shorter lifetime of the multi-droplets. It should be also noted that any contour levels approaching unity exhibit the characteristics of single droplet burning. Any level less or greater than unity implies that multi-droplets vaporization process is slower or faster than single droplet vaporization.

As discussed, the percentage variation in the burning rate of the first and third droplets is within 15% for the 21% O_2 case and within 40% for the 35% O_2 case; see Fig. 15a, c, d, and f. Certainly, the variation margin is larger when the oxygen mole-fraction is larger. These variations are much higher for the second droplet as its margin reaches up to $\sim$ 45% for the 21% O_2 case and up to $\sim$110% for the 35% O_2 case; see Fig. 15b and e. It is clear that the burning rates of the first and third droplets approach unity when $S/r_0 \to 14$, as they recover the burning characteristics of a single droplet at larger S. As for the second droplet, its dimensionless burning rate hardly approaches unity within the range of $4 < S/r_0 < 15$ considered herein and, thus, it is presumed that a very large value of S would be

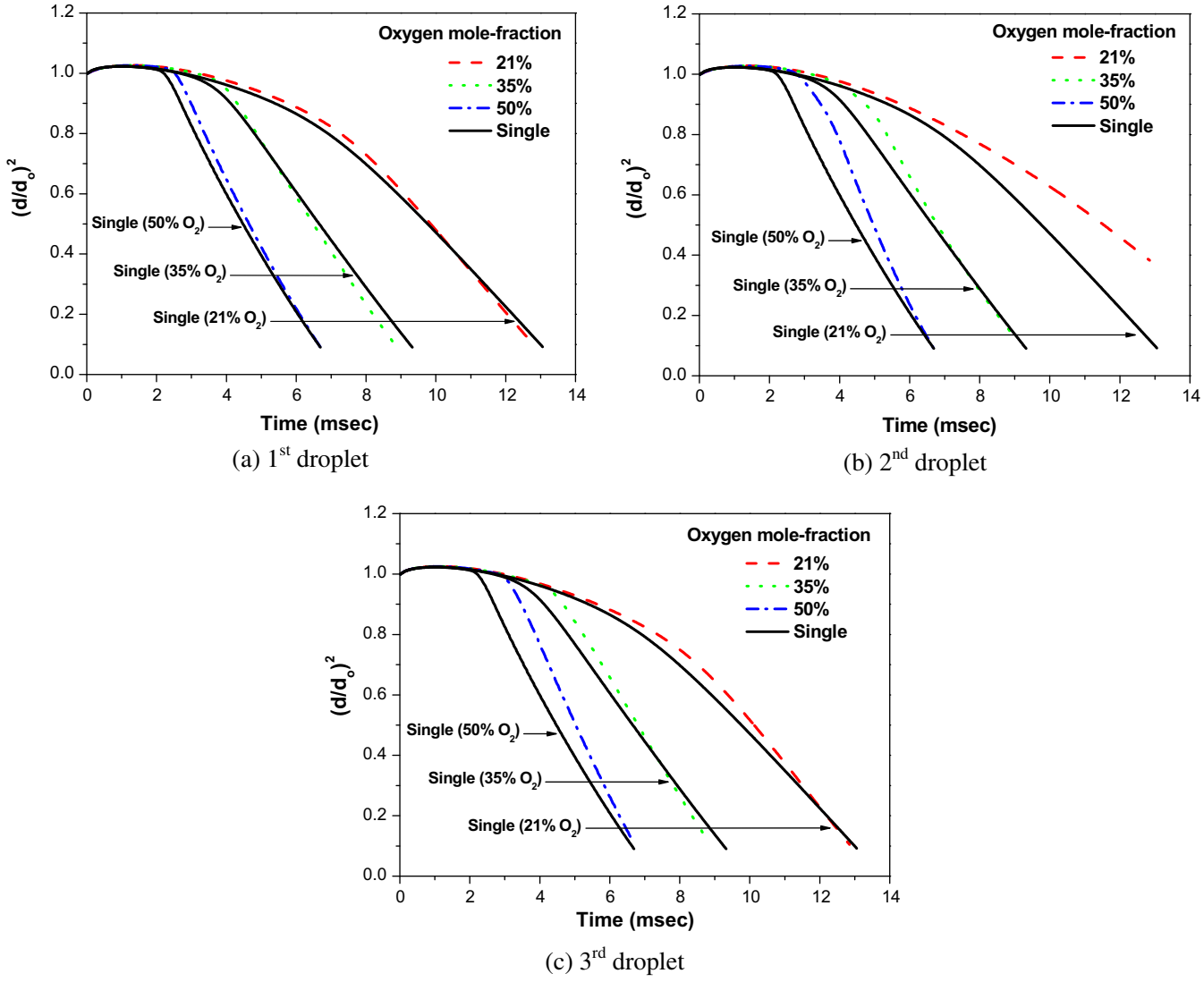

Fig. 14. Histories of the multiple droplet diameter-squared at various oxygen mole-fractions. The separation distance and the oxygen mole-fraction are fixed at $S/r_0 = 4$ and $Re = 10$.

required if the second droplet were to behave like a single droplet. As such, the second droplet is most influenced by the separation distance, S. Generally, when S is small (i.e., $S/r_0 \sim 4$), the cooling by the low-temperature vapor from upstream reduces the vaporization rate of the second droplet and thus the dimensionless burning rate is less than unity. On the other hand, when S is larger, the second droplet burns faster for most Reynolds numbers due to heat added by the flames from upstream; see Fig. 15b and e. These patterns are more prevalent when the Re is relatively large (i.e., $Re \geqslant 30$). When the Re is relatively low (i.e., $Re \leqslant 30$), the variation of S does not yield a significant variation in the burning rate, especially when the oxygen mole-fraction is high; see Fig. 15e.

As previously discussed in Fig. 11, the burning rates of the first and third droplets are essentially determined by two competing mechanisms of heat addition and convection when the separation distance, S, is small. The flames closely located to the droplets add the heat. Convection drives the vaporization as well as shifting of flames and relatively colder vapors downstream.

When Re is very low (i.e., $Re = 10$), the flame entirely surrounds the droplets, which then vaporize. However, when Re is increased to, let us say, $Re = 20$ from Fig. 15a, the front flames disappear because of flame drifting by moderate convective force and thus the burning rate is reduced. When Re is further increased to $Re = 30$ or larger, convection alone essentially drives the vaporization process without downstream-flames affecting the vaporization process of the first and third droplets located in the upstream. This reversal pattern in the burning rate is shown in Fig. 15a and c for the 21% oxygen mole-fraction case; the burning rate is at the lowest when $Re_{crit} = 20$. As for the 35% O_2 case, this reversal pattern is more widespread or occupies a larger area in the S domain, as shown in Fig. 15f. This reversal point of Re_{crit}, defined as the point at which the burning rate is at the lowest, is shifted toward higher values of Re_{crit}.

5. Conclusions

The group combustion of interacting heptanes liquid droplets were numerically simulated by solving two dimensional unsteady laminar Navier–Stokes equations. The unsteady computations for the time-varying vaporization of multi-droplets were carried out with parameters of the Reynolds number (Re), the separation distance (S) between droplets, and the oxygen mole-fraction. The n-heptane droplets initially at $T_0 = 300$ K were in hot air of 10 atm

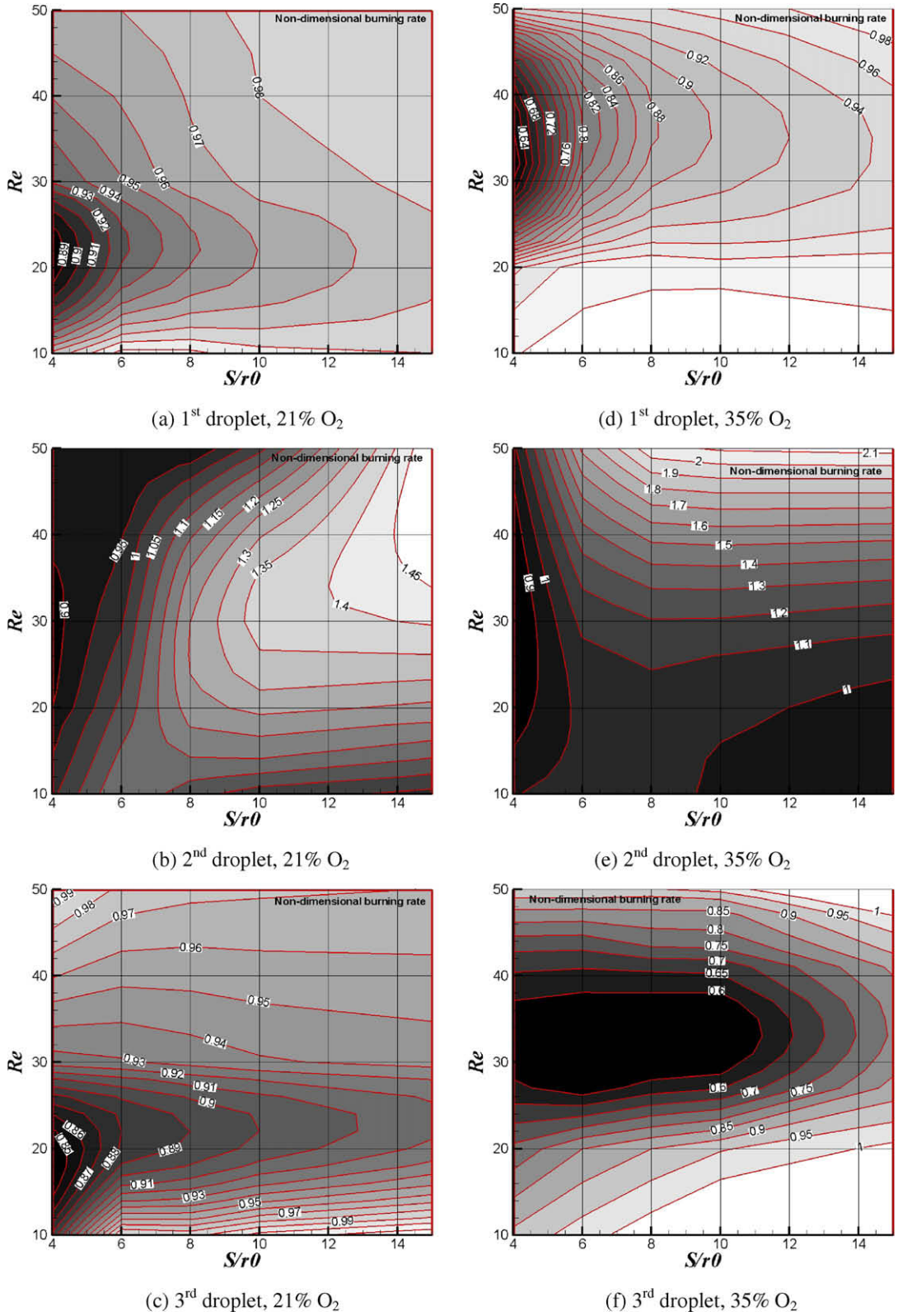

Fig. 15. The dimensionless burning rate of the 1st, 2nd, and 3rd droplets as a function of separation distance (S/r_0) and Reynolds number (Re) for the oxygen mole-fraction of 21% in (a)–(c) and 35% in (d)–(f). The burning time is non-dimensionalized by the single droplet burning rate. The higher the rate, the shorter the lifetime.

and T_g = 1250 K. The multi-droplets staggeringly arranged themselves at a separation distance ranging from 4 to 15 droplet radius. The Reynolds number, based on the droplet diameter and free stream velocity, was varied from Re = 10 to 50. The oxygen mole-fraction of the surrounding air was changed from 15% to 90%. The vaporization process was essentially governed by two competing forces between convection and flame heat addition. When flames were near droplets, heat addition drove the vaporization process; when convection was dominant, gas momentum tended to drift the flames downstream and convection governed the

vaporization process. Moreover, the relatively cold vapors from upstream droplets substantially affected the vaporization process of the droplet downstream. When the oxygen mole-fraction was high, the adiabatic temperature increased, which in turn made the droplets burn faster and the flames closely attach to the droplets.

Acknowledgement

This research was supported by the Combustion Engineering Research Center (CERC) of Korea.

References

[1] Ranz WE, Marshall WR. Evaporation from drops: part I. Chem Eng Prog 1952;48:141–6.
[2] Ranz WE, Marshall WR. Evaporation from drops: part I. Chem Eng Prog 1952;48:173–80.
[3] Miller RS, Harstad K, Bellan J. Evaluation of equilibrium and non-equilibrium evaporation models for many-droplet gas–liquid flow simulations. Int J Multiphase Flow 1998;24:1025–55.
[4] Bellan J, Harstand K. Analysis of the convective evaporation of nondilute clusters of drops. Int J Heat Mass Transfer 1987;30:125–36.
[5] Bellan J, Harstand K. The details of the convective evaporation of dense and dilute clusters of drops. Int J Heat Mass Transfer 1987;30:1083–93.
[6] Yuen MC, Chen LW. On drag of evaporating liquid droplets. Combust Sci Technol 1976;14:147–54.
[7] Wong SC, Lin AR. Internal temperature distributions of droplets vaporizing in high-temperature convective flow. J Fluid Mech 1992;237:671–87.
[8] Downing CG. The evaporation of drops of pure liquids at elevated temperatures: rates of evaporation and wet-bulb temperature. AIChE J 1966;12:170–766.
[9] Thau RT, Lee DN, Sirignano WA. Periodic-solutions of heat transfer for flow through a periodic assemblage of spheres. Int J Heat Mass Transfer 1984;27:1414–7.
[10] Raju MS, Sirignano WA. Interaction between two vaporizing droplets in an intermediate Reynolds number flow. Phys Fluids A Fluid Dynam 1990;2:1780–96.
[11] Chiang CH, Sirignano WA. Interacting, convecting, vaporizing fuel droplets with variable properties. Int J Heat Mass Transfer 1993;36:875–86.
[12] Chiang CH, Sirignano WA. Axisymmetric calculations of three-droplet interactions. Atomization Spray 1993;3:91–107.
[13] Chiu HH, Kim HY, Croke EJ. Internal group combustion of liquid droplets. Nineteenth symposium (international) on combustion, vol. 19. Pittsburgh: The Combustion Institute; 1982. p. 971–80.
[14] Chiu HH, Su SP. Theory of droplets (II): states, structures, and laws of interacting droplets. Atomization Spray 1997;7:1–32.
[15] Prakash S, Sirignano WA. Theory of convective droplet vaporization with unsteady heat transfer in the circulating liquid phase. Int J Heat Mass Transfer 1980;23:253–68.
[16] Akamatsu F, Mizutani Y, Katsuki M. Group combustion behavior of droplets in a premixed-spray flame. Atomization Spray 1997;7:199–218.
[17] Chen G, Gomez A. Dilute laminar spray diffusion flames near the transition from group combustion to individual droplet burning. Combust Flame 1997;10:392–404.
[18] Peng DY, Robinson DB. A new two-constant equation of state. Ind Eng Chem Fundam 1976;15:53–64.
[19] Westbrook CK, Dryer FL. Simplified reaction mechanisms for the oxidation of hydrocarbon fuels in flames. Combust Sci Technol 1981;27:31–43.
[20] Cussler EL. Diffusion mass transfer in fluid systems. Cambridge; 2002 [chapter 3].
[21] Ambrose D, Ghiasses NB. Vapour pressures and critical temperatures and critical pressures of some alkanoic acids: C_1 to C_{10}. J Chem Thermodyn 1987;19(5):505–17.
[22] Doormal JP, Raithby GD. Enhancements of the SIMPLE method for predicting incompressible fluid flows. Numer Heat Transfer 1984;7:147–63.
[23] Constanceau M, Bouard R. Experimental determination of the main features of viscous flow in the wake of a circular cylinder in uniform translation steady flow. J Fluid Mech 1977;79:231–56.
[24] Rengel JE, Sphaier SH. A projection method for unsteady Navier–Stokes equation with finite volume method and collocated grid. Hybrid Methods Eng 1999;1(4):31–56.
[25] Wanderley JBV, Levi CA. Validation of a finite difference method for the simulation of vortex-induced vibrations on a circular cylinder. Ocean Eng 2002;29:445–60.
[26] Brandes E, Hirsch W, Stolz T. Autoignition temperatures for mixtures of flammable liquids with air at elevated pressures. In: Proceedings of the European combustion meeting, Louvain-la-Neuve, Belgium; April 2005.
[27] Rackett HG. Equation of state for saturated liquids. J Chem Eng Data 1970;15(4):514–7.
[28] Latini G, Pacetti M. The thermal conductivity of liquids. Therm Conduct 1997;14:245.
[29] Sastri SRS, Rao KK. A new group contribution method for predicting viscosity of organic liquids. Chem Eng J 1992;50:9–25.
[30] Lemmon EW, McLinden MO, Friend DG. Thermophysical properties of fluid systems. In: Mallard WG, Linstrom PJ, editors. NIST chemistry webbook, NIST standard reference database number 69. Gaithersburg, MD: National Institute of Standard Technology; November 1998.
[31] Thek RE, Stiel LI. A new reduced vapor pressure equation. AIChE J 1966;12:599–602.
[32] Abramzon B, Sirignano WA. Droplet vaporization model for spray combustion calculations. Int J Heat Mass Transfer 1989;32(9):1605–18.
[33] Wilke CR, Lee CY. Estimation of diffusion coefficients for gases and vapours. Indust Eng Chem 1955;47:1253–7.
[34] Lucas K, Abschnitt DA. Berechnungsmethoden fur Stoffeigenschaften. Dusseldorf: Verein Deutscher Ingenieure; 1984.
[35] Poling BE, Prausnitz JM, O'Connell JP. The properties of gases and liquids. New York: McGraw Hill; 2001.
[36] Fuler EN, Ensley K, Giddings JC. Diffusion of halogenated hydrocarbons in helium: the effect of structure on collision cross sections. J Phys Chem 1969;73:3679.